15 Apr 2019

Modeling And Experimental Determination Of Physical Properties Of Ge x -Ga y -Se 1-x-y Chalcogenide Glasses I: Structure And Mechanical Properties

Jason Lonergan

Charmayne Lonergan
Missouri University of Science and Technology, clonergan@mst.edu

John McCloy

Kathleen A. Richardson

Recommended Citation

J. Lonergan et al., "Modeling And Experimental Determination Of Physical Properties Of Ge x -Ga y -Se 1-x-y Chalcogenide Glasses I: Structure And Mechanical Properties," *Journal of Non-Crystalline Solids*, vol. 510, pp. 192 - 199, Elsevier, Apr 2019.
The definitive version is available at https://doi.org/10.1016/j.jnoncrysol.2019.01.031

Journal of Non-Crystalline Solids 510 (2019) 192–199

Contents lists available at ScienceDirect

Journal of Non-Crystalline Solids

journal homepage: www.elsevier.com/locate/jnoncrysol

Modeling and experimental determination of physical properties of Ge_x-Ga_y-Se_{1-x-y} chalcogenide glasses I: Structure and mechanical properties

Jason Lonergan[a,b,*], Charmayne Lonergan[c], John McCloy[b], Kathleen A. Richardson[a]

[a] College of Optics and Photonics, Department of Materials Science and Engineering, University of Central Florida, Orlando, FL 32816, United States
[b] School of Mechanical and Materials Engineering, Washington State University, Pullman, WA 99164, United States
[c] Energy and Environment Directorate, Pacific Northwest National Laboratory, 902 Battelle Blvd., Richland, WA 99352, United States

ABSTRACT

A series of ten $Ge_xGa_ySe_{1-x-y}$ glasses within the topological constraint regime of $< r > = 2.3$ to 2.8 were processed for physical property testing to compare measured to calculated property values enabling further understanding of structure-related mechanical property evolution. Average bond energies were calculated for each glass to elucidate structure and property relationships. Raman analysis was performed to correlate the topological constraint theory to experimentally determined structural units. Young's modulus and Vickers hardness, respectively, were shown to increase with increasing coordination number from 14.42 GPa and 911 MPa at $< r > = 2.4$ to 29.44 GPa and 2295 MPa at $< r > = 2.8$. Poisson's ratio decreased linearly with increasing coordination number from 0.2996 at $< r > = 2.4$ for $Ge_{0.15}Ga_{0.05}$ $Se_{0.85}$ to 0.2477 at $< r > = 2.8$ for $Ge_{0.25}Ga_{0.15}Se_{0.60}$. These properties indicate a strong dependence on the topological network of the glass, in which continued crosslinking and interconnectivity lead to a direct increase or decrease of the respective mechanical property. It was found that theoretical values were in good agreement with measured experiment values, elucidating the impact of the energy required to propagate a crack tip or alter bond lengths and atom positions.

1. Introduction

Chalcogenide glasses (ChGs) are non-oxide glasses that typically combine group 16 elements from the periodic table with group 13 through 15 elements. Applications for these glasses include products such as infrared lenses, fibers, windows, and filters for thermal imaging systems [1]. ChGs typically have large glass forming regions which allows for tailoring of physical properties over a large range of compositions. The chalcogenide elements (S, Se, Te) tend to form covalently bonded chain structures connected to the modifier atoms by weak van der Waals bonds forming layer-like structures. The glass' physical properties are dictated by the glassy structure's local coordination, unique for each composition, making it important to understand the structure-property correlations in order to design optimal chalcogenide glasses for specific applications [2,3]. Specifically, the $Ge_xGa_ySe_{1-x-y}$ glass system is especially attractive to application areas that seek to utilize its broad short- to longwave infrared (IR) transmission, potential for conversion to a glass ceramic, as well as its suitability to rare earth ion doping enabled by the presence of Ga which enhances dopant solubility. Efforts to exploit and extend such use of the glass benefit from a more complete understanding of how the glass chemistry, its bond energies and structure, can be related to physical properties.

The organization of covalent network glasses has been discussed by Phillips and colleagues in terms of a balance of constraints and degrees of freedom [4–7]. The structure-property relationships of Ge_xSe_{1-x} and $Ge_xGa_ySe_{1-x-y}$ glasses have been described as consisting of a network in which the connectivity is controlled by atomic coordination numbers [2,3,8–10]. The fundamental metric used to describe the covalent network topology is the average coordination number, here denoted $< r >$, where (f_i) is the atomic fraction of a given component and (m_i)is the element's coordination number [11].

$$\langle r \rangle = \sum_i f_i m_i \tag{1}$$

The coordination number in ChGs is determined by the "8-N" rule, where N is the number of valence electrons [4,12,13]. There are two important topological thresholds that appear in ternary chalcogenide glasses. The first threshold is the topological percolation threshold, $< r > = 2.4$, that separates the under-constrained region ($< r > < 2.4$) and the over-constrained region ($< r > > 2.4$). The second threshold is the chemical threshold at $< r > = 2.67$, which represents an average transition region from a selenium-excessive composition to a selenium-deficient composition for most chalcogenide compositions. Typically, Ge-based binary and ternary glasses do not show property extrema at $< r > = 2.4$, but rather at $< r > = 2.67$, which represents the tie-line compositions [11]. Tanaka [14] suggested the concept of a network dimensionality (D) associated with $< r >$ values. For $< r > = 2$ in materials like glassy selenium, dimensionality is one (i.e., 1-D) and the

* Corresponding author at: College of Optics and Photonics, Department of Materials Science and Engineering, University of Central Florida, Orlando, FL 32816, United States.
E-mail address: Jason.lonergan@pnnl.gov (J. Lonergan).

https://doi.org/10.1016/j.jnoncrysol.2019.01.031
Received 9 October 2018; Received in revised form 12 December 2018; Accepted 6 January 2019
Available online 26 February 2019

resulting structure is polymeric and chain-like. At $< r > = 2.67$, a fully developed, layer-like 2-D structure exists in the form of tetragonal corner sharing units. As $< r >$ continues to increase, the system moves toward a more crystalline-like, interconnected 3-D network. This crystalline network is completed at $< r > = 4$; such a structure is evidenced by crystalline germanium, a diamond cubic structure where every Ge atom has four neighbors in a tetrahedral arrangement. Recent first-principle and Newtonian molecular dynamics studies on Ge_xSe_{1-x} glass have shown that the simple coordination-based topological models discussed so far can be rigorously applied and provide great insight into the properties of these materials [15–17].

In many estimations of physical properties, a weighted summation is carried out over the individual bond energies, $< E >$, after making some assumptions about what the local distribution of atoms are that comprise the bonds. For example, $GeSe_2$ would have only Ge—Se bonds, where a Se-rich Ge glass would contain some fraction of Se—Se bonds which could be estimated from the stoichiometry. Several lists of bond energies have been used in the past including that of Sanderson [18]. T_g has been shown to correlate well with mean bond energy $< E >$ in covalent glasses, and was shown to relate to the activation energy for viscous flow in an Arrhenius viscosity equation [19]. It has been shown in Ge—Se glasses, that estimates of the surface energy required for bond breaking processes using bond energies, and hence a predictor for a glass' fracture toughness, estimate the overall trends and compositional values with surprising accuracy that increases as one approaches the topological threshold [20].

Correlations between coordination number and properties pertaining to the topological structure and average bond energy have been found in other ternary ChG systems, showing either extrema (molar volume, Poisson's ratio, and optical energy gap), or kinks and changes in slope (Young's modulus, bulk modulus, hardness, and glass transition temperature), when these properties are plotted as a function of $< r >$ [11,14,21,22]. Most of the properties that show a change in slope at $< r > = 2.67$ exhibit a linear trend when plotted versus $< E >$. Some properties, such as hardness, seem to have a linear dependence on $< r >$, which intuitively agrees with the increase of mechanical resistance with increased number of atomic constraints. Other work has shown that elastic tensor components, such as C_{11} and C_{44}, show extrema near both $< r > = 2.4$ and $< r > = 2.67$, indicating a dependence on both topological constraints and average bond energy [23]. Over a wide composition range of chalcogenide glasses, hardness has been shown to correlate both with T_g and with $< r >$, and may therefore be a good experimental measure of average bond strength [24]. Unlike hardness, fracture toughness shows a peak in Ge_xSe_{1-x} glasses at $< r > = 2.4$ corresponding to predominantly $GeSe_{4/2}$ structural units and indicating a dependence on $< E >$ [25]. Therefore, it has been shown experimentally that certain mechanical properties depend on topological constraints and others on chemical ordering and bond energy.

The effects of structure on physical properties in chalcogenide glasses containing high concentrations of Ga—Se and Ga—Ga bonds has not been extensively investigated, but analogues can be found in sulfide ChG glass systems where a wide variety of experimental characterization techniques and several ab initio computational methods have been performed [9,26–33]. Regarding structure, bond lengths for Ga—S units are ~2.26–2.27 Å and Ge-S units are 2.21–2.22 Å, indicating slightly higher packing efficiency for GeS_2 units compared to GaS_2 units [28–30]. Active spectroscopic vibrations have been detected between 150 and 450 cm^{-1} with GeS_2 units having a predominant symmetric stretching mode peak at ~350 cm^{-1} which has been shown to mask the weaker GaS_2 peak which is located at slightly lower frequencies (~325 cm^{-1}) [9,29,33–35]. For sulfur-containing chalcogenide glasses, it has been shown that the predominant structural units within the system are $Ge(Ga)S_{4/2}$ tetrahedra with Ge(Ga)—Ge(Ga) ethane-like units present in chalcogen-deficient systems. Similar structures are expected to be present in $Ge_xGa_ySe_{1-x-y}$ chalcogenide glasses due to the isostructural nature of the Se for S substitution in the glass' network.

The purpose of this study was to systematically explore the physical properties of the ternary $Ge_xGa_ySe_{1-x-y}$ glass-forming compositional space at several fixed Ga levels by investigating mechanical and structural properties, and correlating property trends with changes in topology and bond energy as quantified by $< r >$ and $< E >$. Semi-empirical and theoretical calculations of these properties were made to provide additional insight into the structural and chemical nature of these network glasses. This paper is Part I of a series of two papers examining the property evolution in this ternary system. Part I examines glass structure and mechanical properties, whereas Part II presents an analysis of the bonding attributes on thermal and optical properties within the same composition space.

2. Experimental procedures

2.1. Synthesis

High purity elemental starting materials (Alfa Aesar 5 N for Ge, Ga, and Se) were weighed in 25 g batches for each composition and placed inside 10 mm diameter quartz ampoules within a nitrogen purged glovebox. After batching, the ampoules were evacuated to 10^{-3} Torr and sealed with a methane-oxygen torch. The ampoules were then heated to 800 °C at a ramp rate of 2 °C/min. Melts were constantly rocked for 12 h at the maximum temperature to ensure melt homogeneity. The temperature was then lowered to 750 °C, and the ampoules were removed from the furnace and quenched to room temperature with forced air. Two batches were processed for each composition. The first batch was un-annealed and used solely for differential scanning calorimetry (DSC) to determine T_g while the second batch was annealed at 40 °C below its T_g for 12 h to ensure structural relaxation. A Bruker SENTERRA with $\lambda = 785$ nm laser, 1 mW power, was used to obtain the Raman spectra with a resolution of 2 cm^{-1} using an average of 15 scans.

2.2. Mechanical properties

To assess mechanical aspects of the glass structure; density, elastic moduli, hardness, and fracture toughness were determined experimentally.

Elastic moduli were calculated from measurements of the longitudinal, C_L, and transverse, C_T, acoustic wave velocities. Piezoelectric transducers were used to measure the wave velocities using a Panametrics model 500PR Pulser-Reciever with 5 MHz longitudinal (V110) and transverse (V156) wave transducers. Young's modulus, Y, was derived from the following elastic relationship: [36].

$$Y = \rho \frac{3C_L^2 - 4C_T^2}{\left(C_L/C_T\right)^2 - 1} \quad (2)$$

where ρ is the measured density of the material. Shear modulus can be calculated using only the transverse wave velocity as shown below

$$G = \rho C_T^2 \quad (3)$$

and poisson's ratio is derived using both the values of Young's and Shear modulus [1,36].

$$\nu = Y/(2G) - 1 \quad (4)$$

The Archimedes method was used to measure density of the bulk glass by using room temperature water as the submersion medium.

Hardness values were measured by Vickers indentation using a Shimadzu DUH-211S Micro-hardness tester with a Vickers diamond indenter with an angle of 136 degrees between opposite faces and a square base. Loads ranged from 500 to 800 mN with loading rates of 7 to 9 mN/min respectively. Samples were mirror polished with alumina suspensions of 0.25 μm before indentation. The reported Vickers

hardness values, H_v, represents an average of fifteen tests where the values were defined by [37],

$$H_v = \frac{0.4636P}{a^2} \quad (5)$$

where P is the load applied and a is half the mean size of the two measured diagonals.

Fracture toughness was calculated by increasing the load of the micro-harness tester until cracks could be observed growing away from the corners of the indentation. This resulted in a static load of 2000 mN with a loading rate of 13.32 mN/min. Using Griffith-Irwin fracture criteria for a penny shaped crack, the following equation was used to calculate fracture toughness, where c was the half length of the crack generated by indentation [25,38,39].

$$K_c = 0.016\left(\frac{Y}{H_v}\right)^{1/2}\frac{P}{c^{3/2}} \quad (6)$$

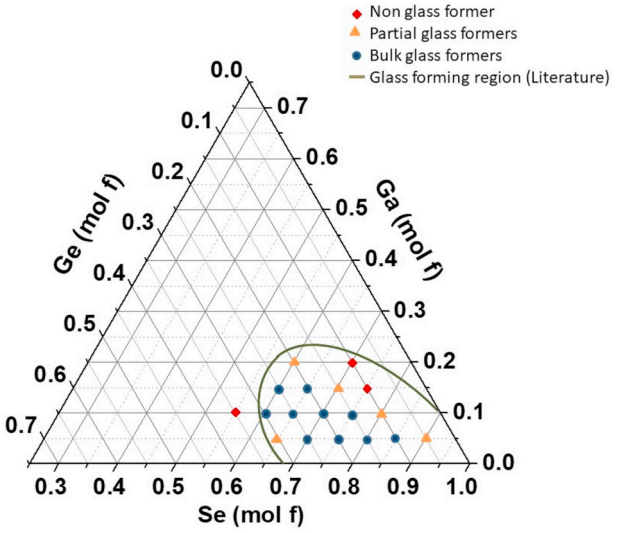

Fig. 1. Ternary diagram of the Ge_x-Ga_y-Se_{1-x-y} system showing non glass formers (red diamonds), glass forming compositions (orange triangles), and the bulk glass formers (blue circles) suitable for physical analysis. In addition, the historical glass forming region as defined by prior literature (green curve) is drawn [8,10]. (For interpretation of the references to colour in this figure legend, the reader is referred to the web version of this article.)

Table 1
Summary of characteristic properties of $Ge_xGa_ySe_{1-x-y}$ glass compositions. All listed values have been calculated directly from the glass' composition, where $< r >$ is the glass coordination number, $< E >$ is the average bond strength, and $\overline{M}$ is the average molecular weight (g/mol).

Ge	Ga	Se	$< r >$	Ge/Se	$< E >$	$\overline{M}$
(at_f)	(at_f)	(at_f)			(eV)	
0.10	0.05	0.85	2.3	0.12	2.22	77.87
0.15	0.05	0.80	2.4	0.19	2.37	77.55
0.20	0.05	0.75	2.5	0.27	2.54	77.23
0.25	0.05	0.70	2.6	0.36	2.73	76.92
0.15	0.10	0.75	2.5	0.20	2.58	77.09
0.20	0.10	0.70	2.6	0.29	2.77	76.77
0.25	0.10	0.65	2.7	0.38	2.99	76.46
0.30	0.10	0.60	2.8	0.50	2.93	76.14
0.20	0.15	0.65	2.7	0.31	3.08	76.31
0.25	0.15	0.60	2.8	0.42	3.02	75.99

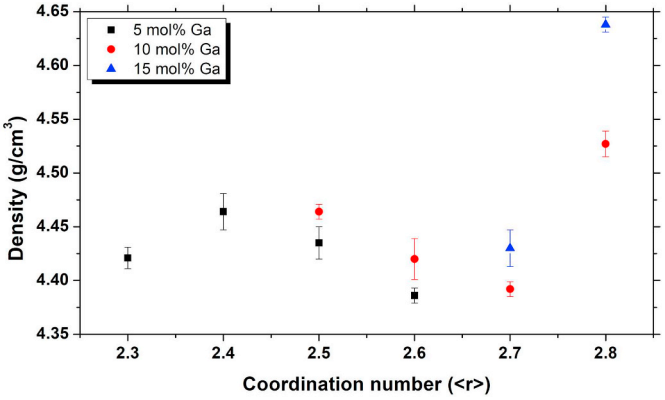

Fig. 2. Density versus coordination number of select $Ge_xGa_ySe_{1-x-y}$ glass compositions that formed good bulk glasses.

3. Results

3.1. Characteristic glass properties

A series of eighteen compositions from 5 to 35 mol% Ge and 5 to 20 mol% Ga were synthesized. Fig. 1 shows the glass-forming region as previously defined by the literature [8,10]. Three symbols were used to identify compositions; non-glass formers (red triangles) were compositions that formed no glass matrix, partial glass formers (orange triangles) were compositions with mixed glassy and crystalline phases, and bulk glass formers (blue circles) were a subset of glass formers that were capable of being scaled to form defect free, 10 mm diameter and 2 mm thick, discs for subsequent property testing. (see Discussion) The glass compositions that formed bulk glass, their equivalent coordination number, and measured characteristic properties are reported in Table 1. XRD (not shown) was used to confirm the glass' amorphous structure with minimal crystallization. Surprisingly, compositions with Ga/Ge > 1 did not form bulk glasses. These glasses formed crystalline compositions when air quenched and reacted violently to higher cooler rates, resulting in the explosion of the quartz ampoule when water quenched. The reason for this reaction is ultimately unknown, but it is postulated that the higher cooling rates caused a large mismatch in thermal expansion coefficients between the glass and the quartz ampoule that resulted in large stresses on the quartz ampoule causing catastrophic brittle failure. Ten of the targeted glasses formed bulk rods that could be cut and polished for subsequent mechanical, optical, and thermal properties testing. This series of bulk-forming glasses covered a span of coordination numbers, $< r >$, from 2.3 to 2.8, spanning both the topological ($< r > = 2.4$) and chemical ($< r > = 2.67$) thresholds, providing sufficient numerical data to study the changes in mechanical, thermal, and optical properties in the $Ge_xGa_ySe_{1-x-y}$ compositional space and are represented by the blue circles in Fig. 1.

Fig. 2 shows the measured density of $Ge_xGa_ySe_{1-x-y}$ compositions from $< r > = 2.3$ to 2.8 (Fig. 3). The lowest density was 4.39 g/cm^3 measured at $< r > = 2.6$, and the highest density was 4.64 g/cm^3 at $< r > = 2.8$. The data has been plotted in three series corresponding to constant Ga mol%, as densities tend to increase with increasing Ga mol %. A maximum is seen at $< r > = 2.4$ as the topological structure transitions from a floppy structure, containing predominantly chain like Se—Se homopolar bonds, to a structure dominated by tetrahedral Ge(Ga)Se_2 units. At the chemical coordination number $< r > = 2.67$, there should be nominally all heteropolar Ge(Ga)—Se bonds. Above $< r > = 2.67$, the density increases as the increase in Ge and Ga content induces Ge(Ga)—Ge(Ga) homopolar bonds, which is the start of over-constrained, more efficiently packed three dimensional ethane-like cage structures. These results are similar to what has been observed in the literature for Ge_xSe_{1-x} systems [2]. Overall, the trends in density can be analyzed by determining the coordination number of the particular

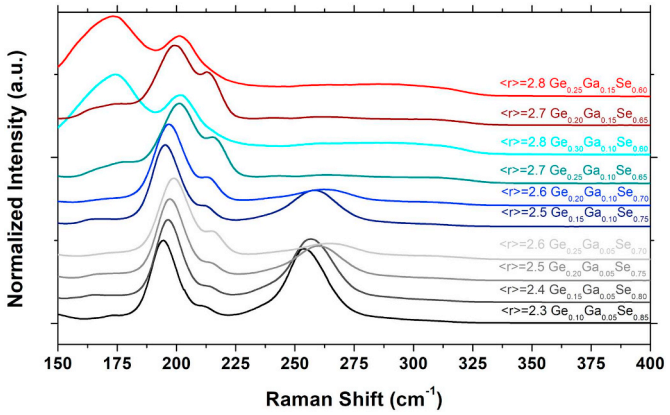

Fig. 3. Raman spectra for $Ge_xGa_ySe_{1-x-y}$ glasses with coordination numbers ranging from $< r \geq 2.3$ to 2.8 using an excitation wavelength of 785 nm.

composition and determining the extent of Se deficiency within the glass relative to stoichiometry.

3.2. Structure

The Raman spectra in this study illustrate spectral features including large bands in addition to several smaller, less well defined, shoulders. Previous studies have attributed the peak near 200 cm^{-1} to the symmetric A1 mode of corner-sharing $GeSe_2$ tetrahedra [9,40,41]. In these tetrahedra, the Ge is connected to four Se atoms and each Se atom is two-fold coordinated. This peak shifts to lower values as Ga content is increased. This is consistent with previous studies that show that Ga—S bonds exhibit less intense signatures than Ge—S bonds at slightly lower (~25 cm^{-1}) Raman shift values [32,42]. This effect is seen within compositions of identical Ga content as peaks shift to higher values as Ge content is increased. Shoulders both to the left (175 cm^{-1}) and right (215 cm^{-1}) of the primary peak are due to stretching of Ge(Ga)—Ge(Ga) bonds in $Se_{3/2}Ge(Ga)—(Ga)GeSe_{3/2}$ ethane-like units, and symmetric in-phase stretching of edge-sharing Ge(Ga)Se_2 tetrahedra in a four-member ring, respectively. It is consistent with topological constraint theory that Ge—Ge ethane-like units (175 cm^{-1}) and edge-sharing (215 cm^{-1}) entities increase with increasing coordination number as the structure becomes increasingly cross-linked and interconnected. The one exception to topological constraint theory is the disappearance of the 215 cm^{-1} shoulder at $< r > = 2.8$ which we partially explain by reference to the role of increasing Ga content with increasing $< r >$. Previous studies have shown that Ga_2Se_3 additions to $GeSe_2$ glasses led to a decreased intensity of the shoulder at 215 cm^{-1} and an increased intensity of the shoulder at 175 cm^{-1}, as well as a small shoulder at 160 cm^{-1} [9]. Although this does not explain the increase in shoulder intensity at 215 cm^{-1} from $< r > = 2.6$ to 2.7 (5 mol to 10 mol% Ga), it does explain the increasing intensity of the 175 cm^{-1} shoulder from $< r > =$ 2.6 to 2.7 (5 to 15 mol% Ga), and the small shoulder observed at 160 cm^{-1} for all compositions. Unique Ga—Se vibrations are not visible as they are hidden due to the more intense Ge—Se vibrations, but glasses with higher Ga content exhibit a shift of the predominant Ge vibratory peaks to lower Raman shift values which is consistent with literature [35,43]. Therefore, all bands attributed to $GeSe_2$ vibrational units may also be attributed to $GaSe_2$ units. The large peaks at 255 cm^{-1} for the low coordination glasses $< r > < 2.7$ are due to Se—Se chains [44–46]. The large peaks disappear above $< r > = 2.7$ as the structure becomes Se-deficient. The broad high-frequency band in region two is due antisymmetric stretching modes of $GeSe_2$ tetrahedra near 300 cm^{-1} as well as out-of-phase stretching of edge-sharing $GeSe_{4/2}$ tetrahedra in four-membered rings near 245 cm^{-1}. The shift of the Se—Se peaks at 255 cm^{-1} to higher values with increasing Ge

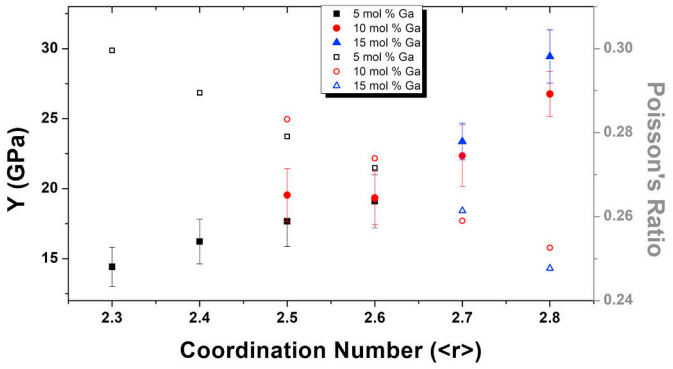

Fig. 4. Young's modulus (solid data points) and Poisson's ratio (open data points) versus coordination number for the $Ge_xGa_ySe_{1-x-y}$ series.

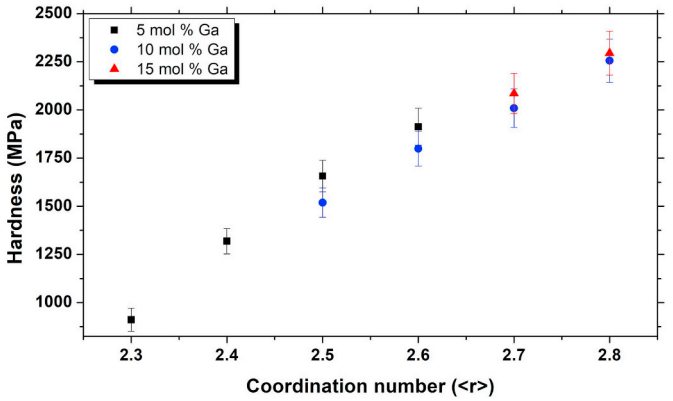

Fig. 5. Vickers hardness values versus coordination number for the Ge_x-Ga_y-Se_{1-x-y} series.

content is most likely due to overlap and coupling of signal with the broad $GeSe_2$ antisymmetric stretching peaks. Overall, the structural interpretation associated with this Raman analysis is consistent with topological constraint theory, showing a 1-D chain like structure at lower coordination numbers (i.e $< r > \approx 2.4$), which is gradually replaced with a more cross-linked 2-D structure (i.e., $< r > = 2.67$) and further crosslinking leads to the development of a 3-D network at higher coordination numbers (i.e., $< r > \approx 2.8$).

3.3. Mechanical

Young's modulus was plotted with Poisson's ratio versus

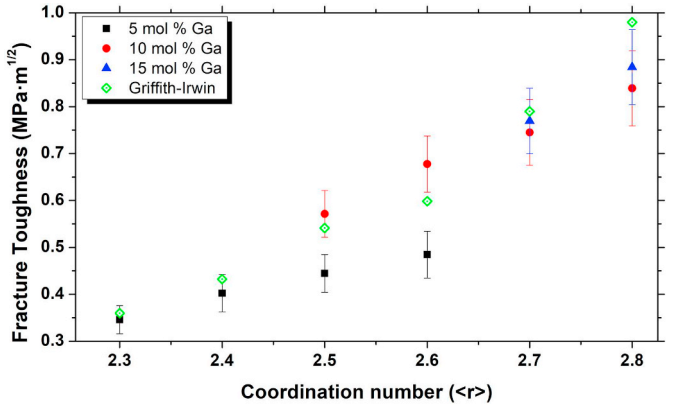

Fig. 6. Fracture toughness of Ge_x-Ga_y-Se_{1-x-y} composition with respect to coordination number from $< r \geq 2.3$ to 2.8. Also shown are the calculated values from Griffith-Irwin theory.

Table 2
Summary of measured physical properties of $Ge_xGa_ySe_{1-x-y}$ glass compositions. All parameters are measured directly or calculated directly from a measured parameter, except K_{IC} and γ which require both measured values and compositional data. C_L and C_T are the measured longitudinal and transverse acoustic velocitites, Hv is the Vicker's hardness, Y is the Young's modulus, ν is Poisson's ratio, K_c is the measured fracture toughness, K_{IC} is the calculated theoretical fracture toughness, and γ is the calculated theoretical surface energy required to break bonds at the crack tip.

Ge	Ga	Se	ρ	C_L	C_T	H_v	Y	N	K_C (MPa·m$^{1/2}$)	K_{IC} (MPa·m$^{1/2}$)	γ/10^5
(at_f)	(at_f)	(at_f)	(g/cm^3)	(m/s)	(m/s)	(MPa)	(GPa)				(J/m^2)
0.10	0.05	0.85	4.42	2096	1121	911	14.42	0.2996	0.346	0.360	2.495
0.15	0.05	0.80	4.46	2198	1196	1319	16.22	0.2895	0.402	0.432	2.664
0.20	0.05	0.75	4.43	2258	1250	1657	17.67	0.2791	0.445	0.508	2.874
0.25	0.05	0.70	4.39	2337	1309	1913	19.10	0.2716	0.485	0.588	3.081
0.15	0.10	0.75	4.46	2374	1306	1519	19.54	0.2832	0.571	0.575	2.941
0.20	0.10	0.70	4.42	2348	1310	1799	19.34	0.2739	0.678	0.608	3.146
0.25	0.10	0.65	4.39	2493	1422	2009	22.35	0.259	0.745	0.758	3.391
0.30	0.10	0.60	4.53	2670	1536	2256	26.76	0.2526	0.839	0.910	3.400
0.20	0.15	0.65	4.43	2544	1446	2086	23.37	0.2614	0.769	0.822	3.517
0.25	0.15	0.60	4.64	2754	1595	2295	29.44	0.2477	0.884	1.050	3.566

coordination, Fig. 4, as the latter is directly related to the first, for the Ge_x-Ga_y-Se_{1-x-y} system. Young's modulus increases with increasing coordination number from 14.42 GPa at $< r > = 2.4$ to 29.44 GPa at $< r > = 2.8$. When compared to the literature, the modulus values for the entire series indicate a relatively soft and malleable glass. For instance, amorphous silica has a Young's modulus of 70 GPa and many rare-earth and oxynitride glasses have moduli in excess of 100 GPa [1]. Modulus increased with increasing coordination number for all samples, except for a small inflection seen in the 10 mol% Ga series around $< r > = 2.6$, suggesting that the stiffness of the glass is a result of the structural topology. There also appears to be a slight increase in modulus for compositions with a higher Ga content.

Poisson's ratio values decrease linearly with increasing coordination number from 0.2996 for $Ge_{0.15}Ga_{0.05}$ $Se_{0.85}$ to 0.2477 for $Ge_{0.25}Ga_{0.15}Se_{0.60}$. No inflection is seen at either the floppy to rigid topological metric of $< r > = 2.4$ or the chemical transition threshold of $< r > = 2.67$. In addition, there does not appear to be significant change in values for composition with similar $< r >$ but different Ge to Ga ratios. These results are consistent with what has been observed in the literature for chalcogenide glasses with values for 1-D chain-like networks approaching 0.35 and decreasing to values around 0.25 for 3-D cage-like networks [1].

Fig. 5 shows the Vickers hardness versus coordination number data, as measured for the $Ge_xGa_ySe_{1-x-y}$ system. These data are summarized in Table 1. Hardness increases with increasing coordination number from 911 MPa at $< r > = 2.4$ to 2295 MPa at $< r > = 2.8$. A nearly linear polynomial trend was observed with increasing hardness for larger coordination numbers. Previous studies on Ge_xSe_{1-x} glasses have exhibited both linear and polynomial trends [25,47]. In our study, no measurable change in Hardness was observed with variations in applied load (across a loading level spanning from 500 to 800 mN). No inflection or shift is seen at either the floppy to rigid transition, $< r > = 2.4$, or the chemical ordering number $< r > = 2.67$. Looking at the three data sets that span the three Ga series examined, no apparent trend is seen regarding the structural impact of the ratio of Ge to Ga suggesting that that the ion's role in the glass network may be isostructural, across this range of compositions.

Fig. 6 shows the fracture toughness versus coordination number for the $Ge_xGa_ySe_{1-x-y}$ system. Overlaid with measured data are those values calculated using Griffith-Irwin theory [38,39,48–50]. The lowest measured value was 0.346 MPa·m$^{1/2}$ for $Ge_{0.10}Ga_{0.05}Se_{0.85}$ ($< r > = 2.3$) and the highest measured value was 0.884 MPa·m$^{1/2}$ for $Ge_{0.25}Ga_{0.15}Se_{0.60}$ ($< r > = 2.8$) as seen in Table 2. These high coordination glass values are relatively high (~55% higher) compared to measured values for Ge_xSe_{1-x} ($< r > = 2.0$ to 2.7, 0.22 MPa·m$^{1/2}$ experimental for $< r > = 2.3$) glasses but compare well to typical oxide glasses (~0.75 MPa·m$^{1/2}$ for soda lime silicate) [25,51,52]. No sharp inflection is seen at either the transition from the floppy to rigid structure, $< r > = 2.4$, or the chemical transition, $< r > = 2.67$. This indicates that the fracture toughness of the glass is a result of the overall structural topology and network connectivity more than average bond strength. Given the linear relationship between bulk mechanical property measurements such as elastic modulus and hardness previously measured and their use in the fracture toughness calculation, the lack of any sharp inflections is not surprising. It should be noted that there are most likely localized changes to flaw population and bulk properties within a nano region around the indenter tip that are not accounted for in Eq. (6) [53]. Fig. 6 also shows an observed fracture toughness increase for compositions with identical coordination number but a higher ratio of Ga to Ge, most likely due to the increased bond strength of the Ga—Se bonds compared to the Ge—Se bonds. It should be noted that previous studies have observed a departure from visco-elastic behavior for certain chalcogen rich glasses in which the T_g is close to room temperature, but this has not been observed in Ge—Se or Ge—X—Se glasses. Therefore, it is unlikely that this is responsible for the decrease in slope of the 5 mol% Ga series [25,47,54].

The apparent indentation fracture toughness values, K_C measured on the glass series were compared to the theoretical Griffith-Irwin similarity principle calculations, K_{IC} (see Appendix A). The theoretical fracture toughness, as determined from computed average bond energy and chemical composition plus measured density and Young's modulus, follow the same trends as the experimental indentation fracture values computed using physical inputs from measured indentation and ultrasonic frequencies (Fig. 6). The increasing fracture toughness from $< r > = 2.3$ to 2.8 corresponds to an increase in network dimensionality and crosslinking.

4. Discussion

The distinction between “bulk glass formers” and “partial glass formers” is important when considering any scale-up of melts to obtain useful sized optical components. We define the “bulk glass formers” region as those quenched and annealed compositions that formed defect-free glasses capable of surviving cutting and polishing procedures when scaled to 25 g melts. Commercially relevant melt sizes are much larger than this and have widely varying thermal histories as compared to those used in the present study. This variation not only impacts resulting glass structure and mechanical properties but more dramatically, the glass' optical properties [55]. “Partial glass formers” consist of those compositions which in a 25 g batch formed a mixed glassy and crystalline phase when forced air quenched but could not be prepared in large specimens due to residual stress and micro cracking that lead to large scale defects when sample machining was attempted. Non-glass formers were 25 g batches that either formed entirely crystalline

microstructures (as determined by XRD) or resulted in ampoule failure during the quenching process.

Understanding the trends in density is difficult, as a monotonic trend does not appear when compared to either topological constraint theory or average bond energy. The decrease in density from $< r > =$ 2.4 to 2.7 corresponds to an increase in connectivity and increase in bond energy. One explanation for this density decrease is the formation of an outrigger raft structure comprised of two edge sharing (ES) tetrahedral connected to four corner sharing (CS) tetrahedral known [56]. In such a network, the ideal ratio of ES to CS tetrahedral occurs at $< r > = 2.4$. At higher coordination numbers, the system becomes over-constrained resulting in less efficiently packed structure and a decrease in density until the emergence of three dimensional cage like units at $< r > = 2.67$. Although this structural paradigm was originally created to explain the structure of Ge_xSe_{1-x} glasses, the inclusion of Ga in the $Ge_xGa_ySe_{1-x-y}$ system into preferential $GaSe_2$ units could lead to a similar tetrahedral network.

The slight inflection in Young's modulus between $< r > = 2.4$ and 2.6 could be due to the reduced packing efficiency of the $Ge_xGa_ySe_{1-x-y}$ system, causing the increase expected in modulus from increased connectivity and bond strength to be offset by the increased volume of structural units. Additionally, a slight increase between glasses with a higher ratio of Ga to Ge for the same $< r >$ is due to the fact that Ga—Se bonds ($U_{Ga\text{-}Se} = 2.32$ eV) are stronger than Ge—Se ($U_{Ge\text{-}Se} = 2.12$ eV) bonds resulting in a more rigid structure [19]. Ultimately, the modulus is predominantly controlled by the connectivity and dimensionality of the glass network, but small changes in properties are observed based on bond strength changes.

Poisson's ratio reflects the resistance of a material to volume change with respect to shape change. It has been shown that it correlates directly to the glass network connectivity and therefore to the dimensionality of the structural units. As Se^{2-} is replaced with either Ge^{4+} or Ga^{4+}, the connectivity of the structure increases, resulting in a lower Poisson's ratio. This is due to the gradual change from a chain-like 1-D polymer structure, to a 2-D structure dominated by tetragonal $Ge(Ga)Se_2$ units, and finally, a 3-D dimensional structure with cage like units. As the structure becomes more connected and higher dimensional, it less capable of stretching or deforming to retain the original volume, indicating a stiffer and more brittle glass. Therefore, Poisson's ratio appears to be controlled by the topological degree of constraint within the glass, as has been reported for other systems [1].

A linear trend is observed when plotting hardness with $< r >$. If average bond strength was the dominant structural factor controlling hardness, one would expect to see a peak at $< r > = 2.67$ due to heteropolar ($U_{Ge\text{-}Sec} = 2.12$ eV and $U_{Ga\text{-}Se} = 2.32$ eV) bonds being stronger than the homopolar ($U_{Se\text{-}Se} = 1.9$ eV, $U_{Ge\text{-}Ge} = 1.63$ eV, or $U_{Ga\text{-}Ga} = 1.48$ eV) bonds present [19]. Therefore, it appears that the hardness of the Ge_x-Ga_y-Se_{1-x-y} composition is primarily dependent on the glass topology and not significantly on the average bond strength. As the structure becomes more interconnected with a higher $< r >$, it becomes more rigid and resistant to physical deformation. These data indicate that hardness is dominated by the network dimensionality and the connectivity of the respective glass forming units, rather than average bond strength alone.

Although the hardness appears to follow a simple linear trend in correlation to bulk structure and topology, it should be mentioned that the indentation process is a complicated process with reversible and irreversible deformation occurring at both bulk and nano scales. Both densification under the tip and shear flow that results in the formation of small mounds at the edges of the residual indenter profile are typically observed [25,53,54]. The amount and ratio of densification and shear flow are compositionally dependent. For instance, structures that are more open, lower density, such as those close to $< r > = 2.67$ have predominantly tetrahedral units which are more resistant to contraction, which could result in higher stress concentration and flaw populations near the indenter tip as well as more shear flow around the edges. For chain like structures, such as those found around $< r > = 2.4$, atomic movement and higher packing efficiencies are possible resulting in more densification at the indenter tip, less residual stress, and less shear flow at the edges. In addition, the indentation method produces high stresses at the tip that could result in localized heating. Increasing temperature tends to relax and restructure glass networks, therefore the hardness and crack propagation properties measured are not truly bulk but a mix of bulk and local mechanisms [53]. With that said, given a series of defect-free samples processed under identical conditions and annealed to remove bulk residual stress, the individual compositions response to these localized mechanisms at the indenter tip is still controlled by the homogenous bonding and topological structure of each glass. Therefore, changes in measured properties, although possibly not true bulk measurements, are still accurate qualitative measurements of the effects of coordination and bonding strength on mechanical behavior.

Fracture toughness exhibits a monotonic trend with $< r >$ although the individual bonds within the Se deficient compositions (Ge—Ge and Ga—Ga) are weaker than the composition composed of primarily heteropolar Ge(Ga)—Se bonds. Thus, it can be envisioned that these 3-D units exhibit more crack-tip blunting than the 1-D Se—Se chain networks or the 2-D tetrahedral networks due to the increased interconnectivity and dimensionality of the ethane-like rings. Similarly, the increased fracture toughness of the $Ge_xGa_ySe_{1-x-y}$ system as compared to the Ge_xSe_{1-x} system could be due to the presence of both $GeSe_2$ and $GaSe_2$ tetrahedral units, which could lead to nano-domain crack-bridging zones within the glass. The jump in fracture toughness predicted by the Griffith-Irwin model from $< r > = 2.6$ to 2.7 is attributable to the Young's modulus increase, which increases ~40% between these two coordination numbers. As mentioned previously, this is most likely due to an increased packing efficiency of the emergent 3-D chain like structure at this point as opposed to the 2-D tetrahedral structure it replaces. The Griffith-Irwin model agrees with the indenter measurements and supports the evidence that overall trends in fracture toughness appear to be dominated by network topology and coordination. Furthermore, the Griffith-Irwin model, calculated with theoretical average bond energy values and bulk Young's modulus measured with non-destructive ultrasonic measurements should be free of any un measured localized change in properties as discussed previously. This suggest that the indenter method, particularly for the $Ge_xGa_ySe_{1-x-y}$ compositional space studied in this paper, is a suitable experimental technique to accurately determine fracture strength and any trends that are connected to glass coordination.

5. Conclusions

A series of eighteen compositions from 5 to 35 mol% Ge and 5 to 20 mol% Ga were melt-quenched, and the ten glasses that formed crystal-free bulk pieces were processed for comprehensive physical property testing of structural and mechanical measurements. Average coordination numbers and bond energies were calculated for each glass to compare physical properties to structure and composition. Raman analysis was performed to correlate the topological constraint theory to experimentally determined structural units. For Se-rich compositions that can be generally considered to be polymeric with Se chains connecting Ge(Ga)-Se structural units, mechanical property values increased with increasing coordination. Acoustic velocities were measured and used to calculate Young's modulus and Poisson's ratio, apparent fracture toughness was measured and compared to calculated fracture toughness using Irwin-Griffith fracture mechanics. All of the measured mechanical properties exhibited a nominally linear behavior with coordination number indicating a strong dependence on the topological network of the glass, in which continued crosslinking and interconnectivity lead to increases in most of these properties. Several properties such as Young's modulus and fracture toughness showed differences in their measured values for compositions with similar

coordination number but varying Ga mol%. Here, an increase in properties was observed that correlated with the glass' increased average bond energy. This indicates that in addition to topology, average bond strength does have some minor effect in regards to the total values in these mechanical properties. Ultimately, this was the first study to thoroughly investigate the structure and mechanical properties of the glass forming region of the $Ge_xGa_ySe_{1-x-y}$ ternary, and specifically interpreting experimentally measured properties considering those predicted using calculated values.

Declaration of interests

The authors declare that they have no known competing financial interests or personal relationships that could have appeared to influence the work reported in this paper.

Acknowledgments

This research was supported in part with funding from the Defense Threat Reduction Agency (DTRA) under Contract No HDTRA1-13-0001. The authors would also like to acknowledge Dr. Anupama Yadav for collecting UV–Vis and XRD data (not shown) used in the paper's preparation.

Appendix A. Theory

A.1. Average bond energy and selenium deficiency

Tichy and Ticha divided compositions into three regions representing deviation from stoichiometric (or perfect chemical ordering), where $R = 1$ is stoichiometric, $R < 1$ is chalcogen-poor (p), and $R > 1$ is chalcogen-rich (r) [19]. In the $R < 1$ region metal-metal homopolar bonds are expected, and in the $R > 1$ region chalcogen-chalcogen homopolar bonds are expected. At $R = 1$, only heteropolar bonds are present, and maxima in T_g are expected due to chemical ordering. The overall mean bond energy is given by Tichy and Tinaka [19] as

$$\langle E \rangle = E_m + E_c \tag{A-1}$$

where E_m is the average bond energy per atom of the non-crosslinked matrix and E_c is the average bond energy of the average crosslinking per atom. The mean bond energy of the average crosslinking per atom E_c is then dependent on the fraction f of the element, its coordination number m, and the bond energy E. [19,58].

$$E_c = P_r E_{hb} = f_{Ge} m_{Ge} E_{Ge-Se} + f_{Ga} m_{Ga} E_{Ga-Se} \; for \; R > 1 \tag{A-2}$$

$$E_c = P_p E_{hb} \; for \; R < 1 \tag{A-3}$$

and E_{hb} is the average heteropolar bond energy given by [19].

$$E_{hb} = (f_{Ge} m_{Ge} E_{Ge-Se} + f_{Ga} m_{Ga} E_{Ga-Se})/(f_{Ge} m_{Ge} + f_{Ga} m_{Ga}) \tag{A-4}$$

Furthermore, E_m is the average bond energy per atom of the remaining matrix [19].

$$E_m = 2(0.5\langle r \rangle - P_r) E_{Se-Se} \langle r \rangle \tag{A-5}$$

where

$$E_m = 2(0.5\langle r \rangle - f_{Ge} m_{Ge} - f_{Ga} m_{Ga}) E_{Se-Se}/\langle r \rangle \; for \; R > 1 \tag{A-6}$$

and

$$E_m = 2\left(\frac{1}{2}\langle r \rangle - P_p\right)\left[\frac{1}{3}(E_{Ge-Ge} + E_{Ga-Ga} + E_{Ge-Ga})\right]/\langle r \rangle \; for \; R < 1 \tag{A-7}$$

Finally, the degree of crosslinking P is defined for chalcogen-rich (P_r, $R > 1$) and chalcogen-poor (P_p, $R < 1$) compositions as [19]

$$P_r = (f_{Ge} m_{Ge} + f_{Ga} m_{Ga})/(f_{Ge} + f_{Ga} + f_{Se}) = 4(f_{Ge} + f_{Ga}) \tag{A-8}$$

$$P_P = (f_{Se} m_{Se} + f_{Ga})/(f_{Ge} + f_{Ga} + f_{Se}) = 2f_{Se} + f_{Ga} \tag{A-9}$$

With definitions for E_c and E_m, one can calculate < E > for any possible composition within the $Ge_xGa_ySe_{1-x-y}$ ternary. Ultimately, the models for < r > and < E > help give insight into observed trends in measured physical properties.

A.2. Fracture toughness

A material's fracture toughness is directly related to the strength of the bonds. In order for a crack to propagate, a tensile force of sufficient strength to exceed the cohesive force of the bonds is required. In addition, a crack can only form or grow if the process results in the total energy of the system remaining constant or decreasing [39,48]. Based on the following two assumptions, Griffith derived a continuum mechanics equation for the fracture stress of a through thickness crack in an infinitely wide plate undergoing brittle facture [39].

$$\sigma_f = \left(\frac{2Y\gamma_S}{\pi a}\right)^{1/2} \tag{A-10}$$

Here Y is the Young's modulus of the material, γ_S is the surface energy per unit area, and a is the length of the crack from the edge of the plate. For certain crack configurations subject to applied loads, it is possible to derive closed-form expressions for the stresses in the body. For mode I stress loading, where the force is applied perpendicular to the direction of the crack, the stress in the x and y direction in place with the crack can be derived as [38,48,50].

$$\sigma_{xx} = \sigma_{yy} = \frac{K_{IC}}{\sqrt{2\pi r}} \tag{A-11}$$

where K_{IC} is the stress intensity factor for mode I loading and r is the radius from the crack tip. The closed-form solution of the stress intensity factor (or fracture toughness) for the through crack in an infinite plate can be derived as [48]

$$K_{IC} = \sigma\sqrt{\pi a} \tag{A-12}$$

Combining Eqs. (A-10) and (A-12), fracture toughness can be expressed as[49]

$$K_{IC} = (2Y\gamma_S)^{1/2} \tag{A-13}$$

The surface energy required to break bonds at the crack tip, γ_S, can be derived as

$$\gamma_S = \frac{1}{2}\frac{1}{N}\langle E\rangle\left(\frac{\rho N_A}{\overline{M}}\right)^{2/3} \tag{A-14}$$

Where, N is the number of atoms per unit volume, < E > is the average bond energy, ρ is density,N_A is Avogadro's number, and $\overline{M}$ is average molecular weight. Therefore, with computational or experimental measurements of the average bond energy, density, chemical composition, and Young's modulus, one could calculate the theoretical fracture toughness of a given glass composition.

References

[1] T. Rouxel, J. Am. Ceram. Soc. 90 (2007) 3019.
[2] G. Yang, T. Gueguen, J.-C. Sangleboeuf, T. Rouxel, C. Boussard-Pledel, J. Troles, P. Lucas, B. Bureau, J. Non-Cryst. Solids 377 (2013) 54.
[3] M. Zhu, Q. Nie, X. Wang, S. Dai, X. Zhang, X. Sehn, G. Wang, X. Lv, Spectrochim. Acta A 75 (2010) 1275.
[4] J.C. Phillips, J. Non-Cryst. Solids 34 (1979) 153.
[5] J.C. Phillips, Physica Status Solidi (b), 101 (473) (1980).
[6] J.C. Phillips, M.F. Thorpe, Solid State Commun. 53 (1985) 699.
[7] M.F. Thorpe, D.J. Jacobs, M.V. Chubynsky, J.C. Phillips, J. Non-Cryst. Solids 266-269 (2000) 859.
[8] A. Giridhar, S. Mahadevan, J. Non-Cryst. Solids 126 (1990) 161.
[9] A.W. Mao, B.G. Aitken, R.E. Youngman, D.C. Kaseman, S. Sen, J. Phys. Chem. B 117 (2013) 16594.
[10] Sudha Mahadevan, A. Giridhar, Jounal of Non-Crystalline Solids 152 (1993) 42.
[11] A.K. Varshneya, A.N. Sreeram, D.R. Swiler, Phys. Chem. Glasses 34 (1993) 179.
[12] J.Z. Liu, P.C. Taylor, Solid State Commun. 70 (1989) 81.
[13] N.F. Mott, Philos. Mag. 19 (1969) 835.
[14] K. Tanaka, Phys. Rev. B 39 (1989) 1270.
[15] M. Micoulaut, A. Kachmar, M. Bauchy, S. Le Roux, C. Massobrio, M. Boero, Phys. Rev. B 88 (054203) (2013).
[16] M. Micoulaut, J.C. Phillips, Phys. Rev. B 67 (2003) 104204.
[17] M. Micoulaut, J.C. Phillips, J. Non-Cryst. Solids 353 (2007) 1732.
[18] K.J. Rao, R. Mohan, Solid State Commun. 39 (1981) 1065.
[19] L. Tichý, H. Tichá, J. Non-Cryst. Solids 189 (1995) 141.
[20] J.-P. Guin, T. Rouxel, J.-C. Sangleboeuf, I. Melscoët, J. Lucas, J. Am. Ceram. Soc. 85 (2002) 1545.
[21] A.N. Sreeram, A.K. Varshneya, D.R. Swiler, J. Non-Cryst. Solids 128 (1991) 294.
[22] Benn Gleason, Laura Sisken, Charmayne Smith, K. Richardson, Int. J. Appl. Glas. Sci. 7 (2016) 374.
[23] S. Mahadevan, A. Giridhar, J. Non-Cryst. Solids 110 (1989) 118.
[24] R.J. Freitas, K. Shimakawa, S. Kugler, Chalcogenide Letters, 10 (39) (2013).
[25] J.-P. Guin, T. Rouxel, J.-C. Sanglebouf, J. Am. Ceram. Soc. 85 (2002) 1545.
[26] Steven A. Luksic, Dong-Sang Kim, Wooyong Um, Guohui Wang, Michael J. Schweiger, Wayne W. Lukens, A.A. Kruger, J. Nucl. Mater. 503 (2018) 235.
[27] Qing Jiao, Li Ge, Lini Li, Changgui lin, Guoxiang Wang, Zijun Liu, Shixun Dai, Xu Tiefeng, Q. Zhang, Sci. Rep. 7 (41168) (2017).
[28] James W.E. Drewitt, Philip S. Salmon, Anita Zeidler, Chris J. Benmore, A.C. Hannon, J. Phys. Condens. Matter 29 (2017) 225703.
[29] I. Pethes, V. Nazabal, R. Chahal, B. Bureau, I. Kaban, S. Belin, P. Jovari, J. Alloys Compd. 673 (2016) 149.
[30] M. Micoulaut, A. Kachmar, M. Bauchy, S. Le Roux, C. Massobrio, M. Boero, Phys. Rev. B 88 (054203) (2013).
[31] T.H. Lee, S.I. Simdyankin, J. Hegedus, J. Heo, S.R. Elliott, Phys. Rev. B 81 (2010) 104204.
[32] A. Povolotskiy, T. Ivanova, A. Manshina, Applied Physics A 887 (2009).
[33] Guoping Dong, Haizheng Tao, Xiudi Xiao, Changgui Lin, Xiujian Zhao, S. Gu, Mater. Res. Bull. 42 (2007) 1804.
[34] Changgui Lin, Laurent Calvez, Haizheng Tao, Mathieu Alliz, Alain Moreac, Xianghua Zhang, X. Zhao, J. Solid State Chem. 184 (2011) 584.
[35] A. Povolotskiy, T. Ivanova, A. Manshina, T. Tver'yanovich, S.-K. Liaw, C.-L. Chang, Applied Physics A 96 (2009) 887.
[36] A.S. Birks, P. McIntire, R.E. Green, ASNT Nondestructive Testing Handbook, Vol. 7 Ultrasonic Testing, 2007.
[37] A. International, Standard Test Methods for Vickers Hardness and Knoop Hardness of Metallic Materials (West Conshohocken, PA), (2016).
[38] G.R. Irwin, Fracturing of Metals, American Society for Metals, Cleveland, OH, 1948, p. 147.
[39] A.A. Griffith, Philisophical Transactions, 221(163) (1920).
[40] E.L. Gjersing, S. Sen, B.G. Aitken, Journal of Physical Chemisty C 114 (2010) 8601.
[41] T.G. Edwards, S. S, E.L. Gjersing, J. Non-Cryst. Solids 3 (2012) 609.
[42] L. Petit, N. Carlie, K. Richardson, A. Humeau, S. Cherukulappurath, G. Boudevs, Opt. Lett. 31 (2006) 1495.
[43] L. Petit, N. Carlie, R. Villeneuve, J. Massera, M. Couzi, A. Humeau, G. Boudebs, K. Richardson, J. Non-Cryst. Solids 352 (2006) 5413.
[44] V.N. Bogomolov, V.V. Poborchy, S.G. Romanov, S.I. Shagin, J. Phys. C Solid State Phys. 18 (1985) L313.
[45] Y. Ledemi, S.H. Messaddeq, I. Skhripachev, S.J.L. Ribeiro, Y. Messaddeq, J. Non-Cryst. Solids 355 (2009) 1884.
[46] A.W. Mao, B.G. Aitken, R.E. Youngman, D.C. Kaseman, S. Sen, J. Phys. Chem. B 117 (2013) 16594.
[47] A.N. Sreeram, A.K. Varshneya, D.R. Swiler, J. Non-Cryst. Solids 130 (1991) 225.
[48] T.L. Anderson, Fractue Mechanics (Fundamentals and Applications), Third Edition, Taylor & Francis, Boca Raton, FL, 2005.
[49] D. Broek, Elementary Engineering of Fracture Mechanics (Netherlands), (1989).
[50] G.R. Irwin, J. Appl. Mech. 24 (1957) 361.
[51] J. Gong, Y. Chen, C. Li, Jounal of Non-Crystalline Solids 279 (2001) 219.
[52] A.T. Akono, N.X. Randall, F.J. Ulm, J. Mater. Res. 27 (2011) 485.
[53] T. Rouxel, Philisophical Transaction Royal Society A, 373 (2015).
[54] T. Rouxel, S. Yoshida, Journal of the Ceramic Society 100 (2017).
[55] Anupama Yadav, Andrew Buff, Myungkoo Kang, Laura Sisken, Charmayne Smith, Jason Lonergan, Cesar Blanco, Michael Antia, Megan Driggers, Andrew Kirk, Clara Rivero-Baleine, Theresa Mayer, Andrew Swisher, Alexej Pogrebnyakov, A.R. Hilton Jr., Greg Whaley, Thomas J. Loretz, Anthony Yee, Greg Schmidt, Duncan T. Moore, K. Richardson, Int. J. Appl. Glas. Sci. 10 (2019) 27–40.
[56] R. Golovchak, O. Shpotyuk, S. Kozyukhin, A. Kovalskiy, A.C. Miller, J. Appl. Phys. 105 (2009) 103704.
[58] M. Micoulaut, Comptes Rendus Chimie 5 (2002) 825.